electronics

MDPI

Article

Accuracy and Uncertainty of Position Detection of Moving Objects by Resonator Arrays

Mattia Simonazzi [1], Leonardo Sandrolini [1] and Andrea Mariscotti [2,*]

[1] Department of Electrical, Electronic, and Information Engineering (DEI), University of Bologna, 40136 Bologna, Italy; mattia.simonazzi2@unibo.it (M.S.); leonardo.sandrolini@unibo.it (L.S.)
[2] Department of Electrical, Electronics and Telecommunication Engineering and Naval Architecture (DITEN), University of Genova, 16145 Genova, Italy
* Correspondence: andrea.mariscotti@unige.it

Abstract: Arrays of magnetically coupled resonators have recently been proposed as position sensors for both static and dynamic applications. Despite their promising characteristics, an accurate evaluation of their functioning in non-ideal conditions is fundamental and necessary to adapt them to industrial contexts. This article analyses the accuracy of the position measurement in resonator arrays under system parameter variations. Appropriate parameters for the evaluation of the sensor performance have been discussed and analysed considering non-ideal system components by exploiting the Monte Carlo method.

Keywords: position sensing; inductive position sensor; resonator array; magneto-inductive waves; uncertainty; capacitors

Citation: Simonazzi, M.; Sandrolini, L.; Mariscotti, A. Accuracy and Uncertainty of Position Detection of Moving Objects by Resonator Arrays. *Electronics* **2024**, *13*, 3099. https://doi.org/10.3390/electronics13153099

Academic Editors: Deniss Stepins and Janis Zakis

Received: 15 June 2024
Revised: 30 July 2024
Accepted: 1 August 2024
Published: 5 August 2024

1. Introduction

Position sensing is one of the main functions implemented in control systems for industrial applications. In addition to accuracy, the relevant characteristics are robustness and compatibility with moving parts, as position sensing is commonplace in the transportation sector. Some examples of applications include the positioning of vehicles (e.g., for electric charging, loading/unloading operations, etc.), the alignment of trains and coaches at platforms, and the movement of large and heavy systems in adverse conditions.

There is a wide range of solutions to the problem of moving object position measurement. Ultrasonic sensors are widely used in production and assembly to sense both the presence/absence of objects and their distance, with measuring ranges from tenths of mm to about 1 m [1]; in this case, the declared accuracy includes hysteresis terms (some %) and temperature drift (also about 1% to 2% maximum).

Capacitive and eddy-current sensors are suitable for much shorter ranges with a constraint of size-of-sensor to distance ratio, which would be unsuitable for the studied cases [2]. In addition, these sensing techniques—in particular the capacitive one—are strongly influenced by the presence of conductive dirt.

There are various types of linear position sensors where the main transducing element is a rod. Linear rod transducers can have a rigid or flexible rod with various techniques to read the rod displacement, such as simply resistive (also called "linear potentiometers") [3], based on a variable differential transformer (so-called "LVDT") [4], Hall effect [4], magneto-inductive [3] or magneto-restrictive [5]. They can offer an extended measuring range, usually in the hundreds of mm but in some cases up to several meters and a tenth of meters. The attention is focused on those able to provide such a measuring range. Linearity error is in the order of a fraction of mm, being declared as 0.02% of full scale with a minimum of ±100 µm for the R-Series V RFV sensors of [5], with all other terms of hysteresis and temperature drift much smaller and negligible. This sensor thus represents the best reference among the considered technologies for measuring linear displacement.

Another characteristic to consider is the relative movement of parts over the entire mission of the system, whereas for example the sensing function can be needed only when they are in proximity, as in the case of an electric vehicle approaching a charging pad or a truck moving along a docking area to reach the point of loading/unloading. Sensors based on solidly anchored elements as the moving rods previously discussed are not suitable in this case.

A promising solution is the use of inductive sensors, composed of magnetically coupled parts, where their relative position affects some system parameters [6–9]. The most straightforward implementation is based on coils (wound or printed on PCBs) coupled to other coils or to metal objects and can be arranged in different ways depending on the application [10–12]. Magnetic coupling may be set up and evaluated in different conditions, at low and high frequencies, depending on, e.g., power consumption, ease and accuracy of the parameter measurement, effect of parasitics and relative insensitivity to their variability. An inductive sensor based on a resonator array is considered in this work for translational or rotational movement. It consists of magnetically coupled resonant coils arranged side-by-side to form a one-dimensional array [13] and an external coil coupled to one or more array resonators.

Resonator arrays have been mainly used for low-power applications, in particular consumer electronics [14–17], but have been recently applied to high-power applications, with due attention to the design of the coils and compensation networks [18]. The possibility of using resonator arrays for detecting metallic (or conductive) objects rather than a purposely designed external coil has also been considered; of course, any object can be detected, provided it is equipped with a coil or tag [19–21]. The scenario of Wireless Power Transfer (WPT) is of particular importance because of the increasing number of implementations [22,23] and in all cases the efficiency of the power transfer strongly depends on the accurate positioning of the receiving coil [24–26].

The resonance condition is exploited to have signal transfer along the array with low losses, and as a positive outcome, the system "selects" an almost pure tone with small harmonic distortion. The peculiar behavior of the array input impedance, which is a continuous function of the external coil position, was initially exploited to track the position of electric vehicles (bearing the external coil) in a wireless dynamic charging scenario, where the power coils were those of the resonator array [27]. The algorithm to reconstruct the vehicle position was simple, taking advantage of the unidirectional motion of the vehicle.

Dynamic conditions, such as in Dynamic WPT (or DWPT), deserve special attention for the required rapidity of the electronic system and algorithms, as observed in [26], where settling times become a limiting element, although this occurs at very high speeds above 400 km/h. Using the proposed approach, the position of the external receiving coil was measured accurately also in dynamic conditions. The accuracy can be enhanced by a properly calibrated system and the spatial resolution is theoretically infinite.

Construction techniques may be exploited to reduce weight and parasitics. The selection of the resonance frequency on the one hand determines the physical dimensions of the coils (and the relevance of parasitic terms) and on the other allows the optimization of the input impedance measurement for issues like sensitivity and noise. The structure is very simple and has a limited number of components, so to keep resonator arrays robust and cheap. Figure 1a shows an example of an array of wire coils allowing the circulation of significant current intensity, so that the system can be exploited for both power transfer and position detection at the same time. In Figure 1b, a PCB printed array is depicted, whose coils can have very small dimensions, so they are particularly robust and non-invasive.

Overall, resonator arrays for position sensing operate by exploiting the input impedance function characteristics, which can present unique values for each position of the moving coil or object. To ensure the bijective property, the array parameters (coil resistance, termination impedance and moving coil impedance) have to be suitably chosen. Issues may arise when considering real components, whose values may vary considerably, especially for

capacitors (that are quite sensitive to temperature, in addition to fabrication tolerance). This paper aims at investigating the effect of component non-idealities on the operation of the sensor and effectively evaluating the uncertainty of the measure, to then discuss how the choice of the termination impedance values can help reduce the effect of the non-idealities on the input impedance.

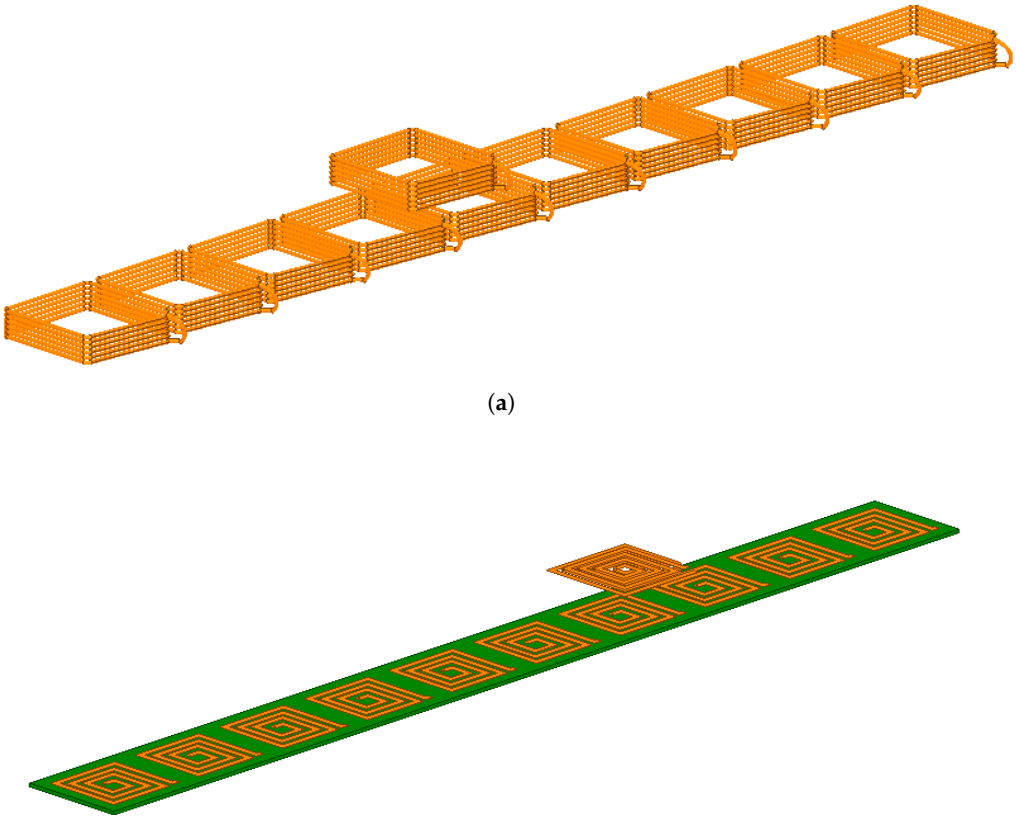

(**a**)

(**b**)

Figure 1. Resonator array made of: (**a**) wound coils and (**b**) printed circuit board spiral coils [28]. It is worth mentioning that the array coils can have different dimensions depending on the designer's choice. Coils wound or printed on PCB can also have the same side length.

The paper is structured as follows. Section 2 recaps the theory of position sensing of moving objects by resonating arrays, including some considerations that will be useful then when discussing circuit behavior, performance and sensitivity. Section 3 provides insight on the circuit parameters that affect performance and that needs to be optimized; it is in fact sensible to analyze the accuracy and uncertainty of the circuit in fair conditions, so set to (almost) optimal conditions. Section 4 focuses on the quantities of interest (the object position and the array input impedance), the sensitivity of the former with respect to the latter and expressions for uncertainty. Section 5 analyses the effect of the variability of the array tuning capacitors and, as a consequence, of the cells resonance and the loops of the impedance curve.

2. Circuit Description

A resonator array made of n identical and evenly spaced coils with an additional resonating coil over it (named "moving coil" or "receiver") is shown in Figure 2. The moving coil position along the array is indicated by x. The mutual inductance terms M between each pair of adjacent coils are the same and we may neglect at a first approximation the

cross-coupling terms between non-adjacent cells, exploiting the "nearest-neighbor approximation" proposed in [14]. The coils have resistance R and self-inductance L, and resonate with a series-connected capacitor of capacitance C at the frequency $f_0 = 1/(2\pi\sqrt{LC})$.

To minimize ohmic losses (especially for high-power applications like DWPT), the coils are usually designed with a large conductor, providing at the same time a large quality factor Q. If the position measurement is not considered integrated with the power transfer function, but separate, then conductors may be much smaller, with a correspondingly lower Q factor. The beneficial effect for the impedance curve separation of a low Q factor was discussed in [28].

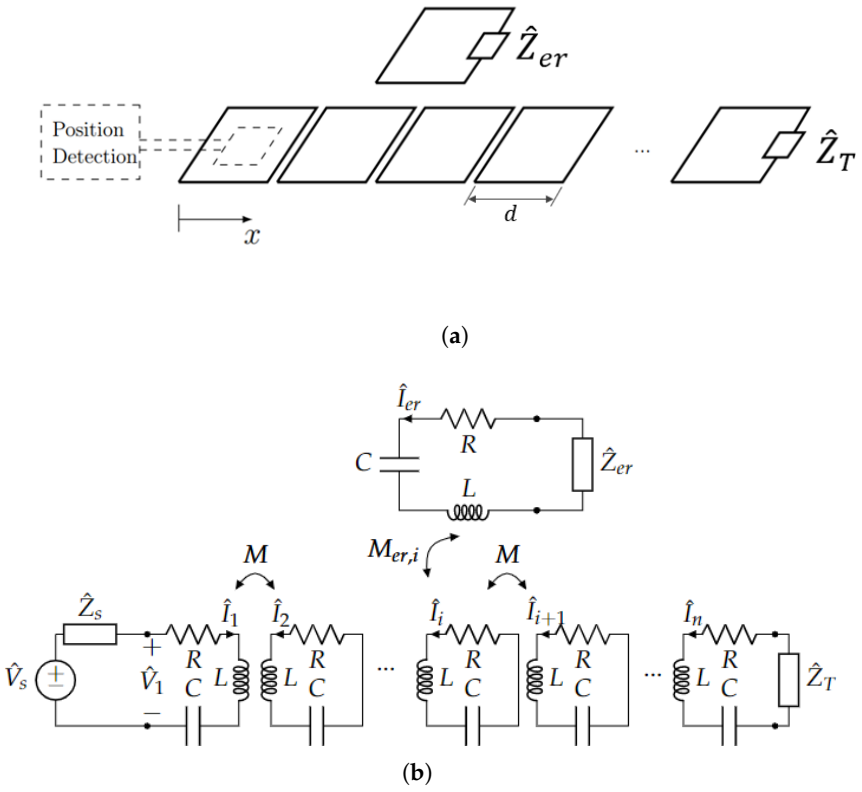

Figure 2. Representation of: (**a**) circuit schematic of a resonator array with an external coil; (**b**) its equivalent circuit [28].

The moving coil is selected as the same length d of the array coils (or slightly smaller), so as to optimize the coupling that can occur with up to two array cells at a time and also allows for "perfect alignment" positions with only one array cell.The mutual inductance term between the moving coil and the generic ith coil of the array, $M_{er,i}$, varies according to the position x. To simplify, a relative coordinate ξ may be defined:

$$\xi = x - (i-1)d \tag{1}$$

where x is the absolute coordinate and i indicates the first array cell coupling with the external resonator while it moves along the array.

For generality and to optimize the impedance behavior, the external coil and the end of the array are loaded by two lumped impedances, $\hat{Z}_{er}$ and $\hat{Z}_T$, respectively (see Figure 2). These impedance terms represent two degrees of freedom to tune the behavior of the system, crucial for the position measurement accuracy.

A sinusoidal input voltage is applied to the first array resonator at its resonant frequency f_0; as a consequence, all currents and voltages are phasors at the same frequency. The impedance of each array resonator is

$$\hat{Z} = R + j\omega_0 L + 1/(j\omega_0 C)\ , \tag{2}$$

whereas $\hat{Z}_T$ and $\hat{Z}_{er}$ must be added to the impedance of the last cell and to that of the external resonator:

$$\hat{Z}_n = R + j\omega_0 L + 1/(j\omega_0 C) + \hat{Z}_T \tag{3}$$

$$\hat{Z}_{er} = R + j\omega_0 L + 1/(j\omega_0 C) + \hat{Z}_{er} \tag{4}$$

In resonant conditions, such expressions reduce to $\hat{Z} = R$, $\hat{Z}_n = R + \hat{Z}_T$ and $\hat{Z}_{er} = R + \hat{Z}_{er}$, respectively.

The electrical behavior of the system can be described with a set of $n + 1$ equations.

$$\begin{aligned}
-\hat{V}_s + \hat{Z}_s\hat{I}_1 + \hat{Z}\hat{I}_1 + j\omega M\hat{I}_2 &= 0\\
j\omega M\hat{I}_1 + \hat{Z}\hat{I}_2 + j\omega M\hat{I}_3 &= 0\\
\vdots &\ \vdots\\
j\omega M\hat{I}_{i-2} + \hat{Z}\hat{I}_{i-1} + j\omega M\hat{I}_i &= 0\\
j\omega M\hat{I}_{i-1} + \hat{Z}\hat{I}_i + j\omega M\hat{I}_{i+1} + j\omega M_{i,er}(\xi)\hat{I}_{er} &= 0\\
j\omega M\hat{I}_i + \hat{Z}\hat{I}_{i+1} + j\omega M\hat{I}_{i+2} + j\omega M_{i+1,er}(\xi)\hat{I}_{er} &= 0\\
j\omega M\hat{I}_{i+1} + \hat{Z}\hat{I}_{i+2} + j\omega M\hat{I}_{i+3} &= 0\\
\vdots &\ \vdots\\
j\omega M\hat{I}_{n-1} + \hat{Z}\hat{I}_n + \hat{Z}_T\hat{I}_n &= 0\\
j\omega M_{er,i}(\xi)\hat{I}_i + j\omega M_{er,i+1}(\xi)\hat{I}_{i+1} + \hat{Z}_{er}\hat{I}_{er} &= 0
\end{aligned} \tag{5}$$

The solution of (5) is detailed in [28]. The position of the moving coil affects the KVL equations through the mutual inductance terms $M_{er,i}(\xi)$ and the array input impedance $\hat{Z}_{eq}(x)$, which corresponds to the ratio of input voltage $\hat{V}_1(x)$ and current $\hat{I}_1(x)$ phasors at the frequency f_0:

$$\hat{Z}_{eq}(x) = \frac{\hat{V}_1(x)}{\hat{I}_1(x)} = \frac{\hat{V}_s}{\hat{I}_1(x)} - \hat{Z}_s. \tag{6}$$

Due to the coupled external coil, $\hat{Z}_{eq}(x)$ presents in general complex values also at resonance [27]. The array could be supplied with a current source (constant current value while $\hat{Z}_{eq}(x)$ varies) and the resulting input voltage measured with a simple voltage divider. However, the more intuitive approach with a voltage source and an input current measurement is the one considered in the following.

The input impedance in analytic form can be obtained from (5) by selecting the one referred to the first resonator (by iteratively substituting the equation of the adjacent resonator, starting from the nth one). Thus, (5) reduces to:

$$-\hat{V}_s + \left[\hat{Z}_s + \hat{Z}^{eq}_{i,i+1}(\xi)\right]\hat{I}_1 = 0 \tag{7}$$

where $\hat{Z}^{eq}_{i,i+1}(\xi)$ corresponds to the equivalent impedance at the input of the first cell of the array with the external coil positioned over and thus coupled with the ith and $(i+1)$th coils.

The input impedance has both the magnitude and the phase which oscillate as the external coil moves along the array [27]. In particular, while the magnitude is always

positive, the angle can be either positive or negative, thereby meaning that $\hat{Z}_{eq}(x)$ cycles between inductive and capacitive behavior. For the successful determination of x, $\hat{Z}_{eq}(x)$ must have a one-to-one behavior with it (a so called "bijective" function with a complete mapping between the two domains).

3. Circuit Parameters and Optimization

The coil array circuit, as previously described, has some parameters that represent the degrees of freedom to adapt the circuit to various applications and to optimize its performance, e.g., in terms of spatial resolution and accuracy.

In fact, the proposed sensor lends itself to being scaled and integrated into systems of any size. To ensure accuracy and reliability, it is necessary to consider the size of the components and the operating conditions for the specific application. In fact, there are no standardized reference inductance and resonant frequency values for these sensors, and they need to be evaluated for the specific application. For example, in [11] the target application was the Large Hadron Collider in Switzerland, with an immunity to the external magnetic field as the first and foremost requirement. In [10], some applications are exemplified, among which the measurement of traveled distance of milling and tooling machines, with an emphasis on accuracy and resolution. In [27], the same array of a WPT system was used to support the measurement of the EV position, under the constraints of standardized resonance frequency and limited coil resistance to keep energy efficiency high.

Such parameters of the electric circuit are discussed in the following.

3.1. Coils Resistance and Physical Length

As anticipated, the coil resistance R is usually minimized to reduce power losses, but at the same time low values limit the excursion of the $\hat{Z}_{eq}(x)$ values. In this way, large R values guarantee that $\hat{Z}_{eq}(x)$ values can be distinguished as x varies. In other words, the larger the coil resistance, the larger the attenuation when the external coil moves farther from the array input cell, providing a measurable difference in the $\hat{Z}_{eq}(x)$ loop curves at each new array coil coupled by the moving external coil. Coil resistance minimization is not a requirement of primary importance for an application where the array to sense position is separated from the array to exchange power with the load (as used for example in Wireless Power Transfer (WPT) applications with moving electric vehicles [25,27]).

The coil resistance determines the coil quality factor at resonance, taking into account that the coils are designed to maximise the self and mutual inductance terms. The remaining degrees of freedom are the array coils number n, the coil length d in the x spatial direction and the impedances $\hat{Z}_T$ and $\hat{Z}_{er}$.

Referring to the physical extension to cover with the array length l_x, an arbitrary number of resonators could be used: the higher their number n, the larger the number of complete loops of $\hat{Z}_{eq}(x)$. This in turn improves the position accuracy because, for the same amount of longitudinal movement, the variation of $\hat{Z}_{eq}(x)$ is larger, going through many complete turns of its phase.

From another viewpoint, since the space variation of $M_{er,i}(x)$ is continuous, we could opt for the extreme case of an array made of only one resonator. However, the moving coil length has to be larger than half of the array resonator length, otherwise $M_{er,i}(x)$ would be symmetric with respect to x and it would not be possible to distinguish whether the external moving coil covers the first or second half of a resonator.

3.2. Termination Conditions

The termination impedances $\hat{Z}_T$ and $\hat{Z}_{er}$ are chosen real values, not to alter the coil self-resonance frequency, and they correspond from a general standpoint to the short-circuit (SC), open-circuit (OC) and matching terminations, typically considered for resonator array applications [14]. Three such conditions for clarity correspond to $\hat{Z}_T = 0$, $\hat{Z}_T \to \infty$ and $\hat{Z}_T \approx \omega_0 M$.

The analysis carried out in [28] has confirmed that best performances are obtained for a matching termination condition when the coil presents $Q < 100$. The analysis was carried out on a 10-cell array and always considering two coil factors of merit Q, by checking three different coil resistance conditions ($0.2R_{er}^{opt}$, R_{er}^{opt} and $5R_{er}^{opt}$), having defined

$$R_{er}^{opt} = \omega_0 M_{er,i}^2(x)\big|_{\max} \tag{8}$$

A verification of the input impedance variation for different height values of the moving coil above the array has confirmed that variability is moderate and there are no situations of collapsing or overlapping impedance loops for an order of magnitude of change of such a height [28].

4. Performance and Sensitivity

The system is now considered for what regards the characteristics of the input current dynamic range and of the position accuracy and sensitivity, provided that it was designed and set in an optimized configuration, as discussed in Section 3. The current dynamic range is closely related to the expected value of the input impedance and can be adjusted by acting on the excitation voltage. The basic position accuracy is mainly affected by the number of coils n, which determines the periodicity and therefore the trend of the array input impedance for the given array length l.

It can be noticed that Δx was fixed when the discretization step used to calculate the mutual inductance function $M_{er,i}(x)$ was determined. In case the geometry of the array allows to calculate $M_{er,i}(x)$ in closed form, then ideally $\Delta x \to 0$. The minimum step is to be determined by considering the accuracy of the current sensor and the computational burden (depending in turn on the DSP capability).

Given that $\hat{Z}_{eq}(x)$ is a complex value function, its sensitivity to the space variation Δx is defined for both amplitude and phase at a certain value of the (discretized) space coordinate x_k as the difference quotients:

$$S_{mag}(x_k) = \frac{\Delta|\hat{Z}_{eq}|}{\Delta x}(x_k) \qquad S_{ph}(x_k) = \frac{\Delta\varphi_{\hat{Z}_{eq}}}{\Delta x}(x_k) \tag{9}$$

Intuitively, the larger the value of the $S(\,)$ functions, the larger the accuracy of the measurement. However, if the sensitivity values are too high, the sensor may be required to evaluate extreme values of impedance, resulting in the necessity to cover large dynamics, unnecessarily complicating the measurement system. The sensitivity is mainly affected by the space variation of the mutual inductance $dM_{er,i}(x)/dx$. Once $M_{er,i}(x)$ and Δx have been defined, the number of the array coils n can be chosen according to its length l_x and the desired value of the sensitivity quantities S_{mag} and S_{ph}.

Considering the system operating at resonance, the coil resistance makes the values of the array input impedance different for each moving coil position x. Indeed, while the magnitude or the phase of $\hat{Z}_{eq}(x)$ can assume same values for different x values, their combination is unique to a given x. This can be seen in Figure 3a, that shows the trajectory of the input impedance function in the complex plane versus x, having fixed a value of $\hat{Z}_t$ and $\hat{Z}_{er}$. There are no intersections in the amplitude-phase plot, so that the function is bijective.

The sensitivity parameters for this reference case are shown in Figure 3b.

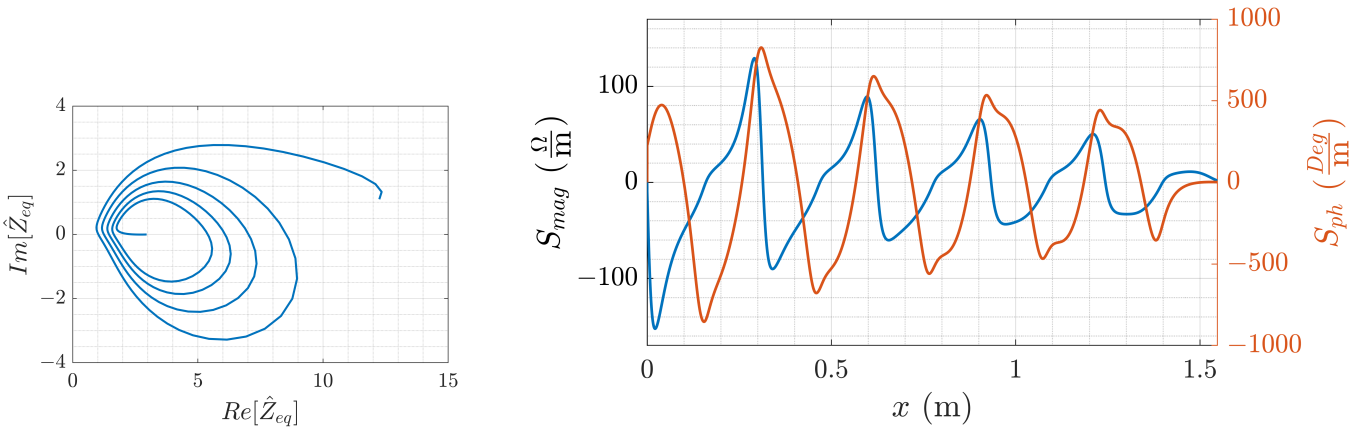

(**a**) (**b**)

Figure 3. Input impedance (**a**) trajectory and (**b**) sensitivity of the 10-cell array as a function of x with matched termination and $\hat{Z}_{er} = Rl_{er}^{opt}$.

Then, comparing the estimated (through the measurement of the input voltage and current) and theoretically calculated values, it is possible to determine the moving coil position x. In particular, the calculated impedance should match the estimated one within a tolerance. The conditions can be written as:

$$\| \widetilde{Z} - |\hat{Z}_{eq}(x)| \| \leq \delta_Z, \tag{10}$$

$$\| \widetilde{\varphi} - \varphi_{\hat{Z}_{eq}}(x) \| \leq \delta_\varphi, \tag{11}$$

where δ_Z and δ_φ fix the tolerance margins for the magnitude and phase quantities.

$\hat{Z}_{eq}(x)$, being a bijective function, has no crossovers and its values are always distinct. This means that it is in principle always possible to determine position x^* with a single measurement with infinite accuracy. Two points must, however, be considered from a practical standpoint:

- $\hat{Z}_{eq}(x)$ is not invertible and the determination of x^* is achieved iteratively [28]; x values are thus discrete (indicated by a sequence x_k), evenly distributed and separated by Δx, that sets the resolution of the longitudinal axis; $\hat{Z}_{eq}(x)$ is thus replaced by $\hat{Z}_{eq}(x_k)$;
- voltage and current measurements at the resonance frequency are unavoidably affected by noise and limited accuracy, for which each measured value is accompanied by a confidence interval.

For the latter, starting from the standard uncertainty of the voltage and current readings at the resonance frequency, $u(\hat{V}_1)$ and $u(\hat{I}_1)$, we can define a corresponding uncertainty for the estimated $\hat{Z}_{eq}$, distinguishing amplitude and phase. Let us indicate the magnitude and phase of $\hat{V}_1$ and $\hat{I}_1$ as V_1 and I_1, and ψ_V and ψ_I, respectively. We know that the amplitude and phase of $\hat{Z}_{eq}$ are determined as:

$$|\hat{Z}_{eq}| = \frac{V_1}{I_1} \qquad \angle\hat{Z}_{eq} = \psi_V - \psi_I \tag{12}$$

Assuming then that the voltage and current measurements are uncorrelated, the uncertainty may be calculated straightforwardly ignoring the crossed terms:

$$u(|\hat{Z}_{eq}|) = u\left(\frac{V_1}{I_1}\right) = \sqrt{\left(\frac{u(V_1)}{V_1}\right)^2 + \left(\frac{u(I_1)}{I_1}\right)^2} \tag{13}$$

$$u(\phi_{\hat{Z}_{eq}}) = u(\psi_V - \psi_I) = \sqrt{(u(V_1))^2 + (u(I_1))^2} \tag{14}$$

The two uncertainty quantities above for magnitude and phase must be then divided by the two sensitivities, in order to derive the expected uncertainty on the position value. This, in turn, determines the minimum acceptable discretizing step Δx. In general, it is required that

$$\begin{cases} \Delta\hat{Z}_{eq} > u(|\hat{Z}_{eq}|) \\ \Delta\varphi_{\hat{Z}_{eq}} > u(\varphi_{\hat{Z}_{eq}}) \end{cases} \quad \forall\ \Delta x \tag{15}$$

The discretization step Δx must be chosen on the one hand as small as possible for a matter of improved spatial resolution and on the other hand aligned with the estimated uncertainty (to avoid wasting calculation power with small spatial resolution that cannot be resolved reliably). In this sense, the minimum Δx value can be set as follows with respect to the estimated uncertainty.

$$\Delta x > \begin{cases} \dfrac{u(|\hat{Z}_{eq}|)}{\min\limits_k\{S_{mag}(x_k)\}} \\ \dfrac{u(\varphi_{\hat{Z}_{eq}})}{\min\limits_k\{S_{ph}(x_k)\}}. \end{cases} \tag{16}$$

It is worth mentioning that in case the required Δx does not satisfy (16), it is possible to increase the number of coils n, so that S_{mag} and S_{ph} increase for the same Δx. It is nevertheless observed that using Δx values comparable or slightly smaller than uncertainty would not lead to unusable information or undetermined position scenarios, only to a poorer quality in the determination of the position.

5. Performance under Uncertain Array Parameters

In practical applications, the actual component values are likely to deviate from the nominal values used during design, with the risk of compromising fine tuning and system operation. The array input impedance might for instance lose its bijective nature.

Based on the authors' experience, capacitors (rather than inductors and resistors) are subject to larger deviations, due to both production tolerance and temperature effect, with typical spreads as high as 10%, and in general never below 1%. In the following, the $\hat{Z}_{eq}$ trajectory vs. x is evaluated for different termination conditions and external coil impedance under capacitance mismatch, using the same test case with 10 cells as in the previous section.

5.1. Example with Non-Ideal C_2, C_5 and C_7 Capacitors

The capacitors inserted in the resonators are named C_i, $i = 1, 2, \ldots, 10$, and by default, $C_i = 1/(\omega^2 L)$; only the mismatched values are explicitly indicated. As a first example, a variation of the second, fifth and seventh capacitance has been applied, applying a uniform distribution for the following spreads: $C_2 = (1 \pm 0.03)C_0$, $C_5 = (1 \pm 0.02)C_0$, $C_7 = (1 \pm 0.05)C_0$, where $C_0 = 1/(\omega_0^2 L)$. The resulting trajectories are plotted in Figure 4 and undergo significant changes.

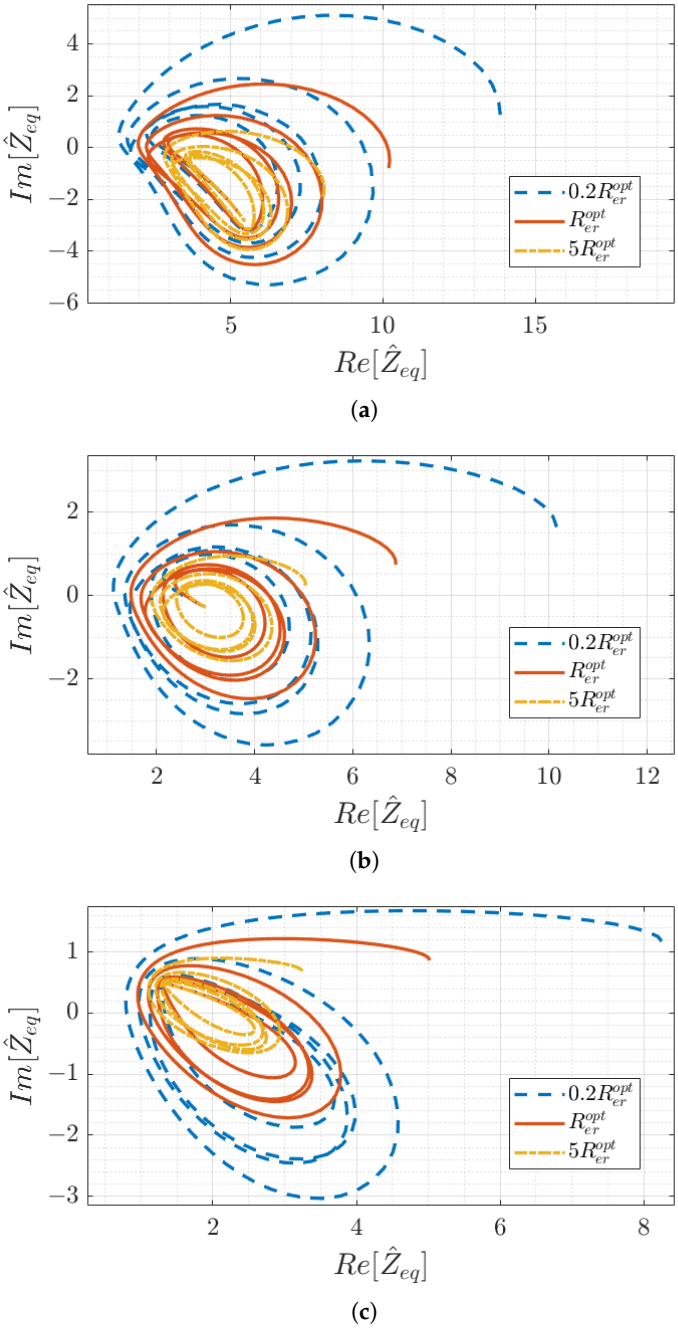

Figure 4. Input impedance trajectories of a 10-cell array with $C_2 = (1 \pm 0.03)C_0$, $C_5 = (1 \pm 0.02)C_0$, $C_7 = (1 \pm 0.05)C_0$ and quality factor $Q = 90$ for different values of load resistance $\hat{Z}_{er}$: (**a**) array terminated in short condition, (**b**) matched condition, and (**c**) open condition.

Indeed, for all the considered terminations, the input impedance trajectory intersects itself and thus the bijective nature of the input impedance function and the sensing operations are compromised.

The optimal configuration shown in Figure 3a cannot be exploited anymore, since the curve intersects as it can be seen from the red curve of Figure 4b. However, by exploiting the system degrees of freedom (the array termination and the external resonator load), it is possible to modify and optimize the trajectory of the input impedance.

5.2. Evaluation of Variability of the Cell Tuning Capacitance

A more consistent evaluation of the effect of each capacitance variation can be performed using the Monte Carlo method. Indeed, the variation of the capacitance of a component can be considered stochastic, being the result of processes affected by many variables that are often not known (especially to the user). It was therefore decided to evaluate the effect of the uncertainty on the parameters by considering the stochastic variation of the capacitors connected to each coil (lumped capacitance). The result is the shift of the cell resonance frequency with respect to the reference one, which may be different for each cell. To verify that the position of the external coil can still be sensed accurately, it is necessary to check that $\hat{Z}_{eq}$ is still bijective, meaning that it should have a different complex value for each position x. This is equivalent to verifying that for each position x_i the following holds:

$$K_i = \left\| \hat{Z}_{eq}(x_i) - \hat{Z}_{eq} \right\| > \delta \tag{17}$$

where δ is a tolerance margin that can be arbitrarily chosen based on the specific system and application.

Indeed, K_i should be greater than the minimum detectable value of the measuring system, set by its sensitivity and uncertainty.

At this point, however, it is necessary to note that the condition (17) must be verified considering the spatial resolution of the device, i.e., the discrete positions x_k that the sensor can actually detect. In fact, from a theoretical point of view, $\hat{Z}_{eq}$ is a continuous function and during the design it can be calculated numerically using tens of thousands of points, resulting in discretization steps in the order of microns.

However, the effective Δx_{eff} that the system can actually detect is limited by the current measurement characteristics, as discussed in Section 3. It must be noticed that $\hat{Z}_{eq}$ must be bijective for the x_k points detected by the sensor and not for every x, allowing the operation provided that the condition (17) is fulfilled at x_k.

The effect of capacitance spread for a specific Δx_{eff} can be evaluated by defining the parameter

$$K_{\hat{Z}_{eq}} = \min_i K_i \tag{18}$$

indicating the minimum value of $\hat{Z}_{eq}$ the system can detect.

Similarly, the parameters $S_{mag,\Delta}$ and $S_{ph,\Delta}$ for a specific Δx have been introduced as:

$$S_{mag,\Delta} = |\max S_{mag} - \min S_{mag}| \tag{19}$$

$$S_{ph,\Delta} = |\max S_{ph} - \min S_{ph}| \tag{20}$$

and provide an indication of the variation extent of S_{mag} and S_{ph} for each Monte Carlo run.

As a case study, the 10-cell resonator array with matched terminations is considered. Their parameters for the ideal case are shown in Figure 3a,b. For a reference, $\Delta x_{eff} = 1\,\text{mm}$, $K_{\hat{Z}_{eq}}$ and the sensitivity parameters $S_{mag,\Delta}$ and $S_{ph,\Delta}$ have been calculated enforcing the capacitance deviates from its datasheet value of a certain amount that is randomly generated from a normal distribution assuming a specific standard deviation u_c.

Specifically, three different sets of 100 Monte Carlo simulations were performed, considering $u_c = 3\%, 5\%, 8\%$ (see Figure 5). The plot of Figure 5a shows that the minimum detection value $K_{\hat{Z}_{eq}}$ to comply with in case of capacitance variability is lower than in the ideal case, thus requiring improved performance for the measuring system. Sensitivity is also affected when considering $S_{mag,\Delta}$ and $S_{ph,\Delta}$, smaller and larger than the ideal case, respectively. This means that the amplitude of $\hat{Z}_{eq}$ is reduced, while the phase makes more turns per unit length.

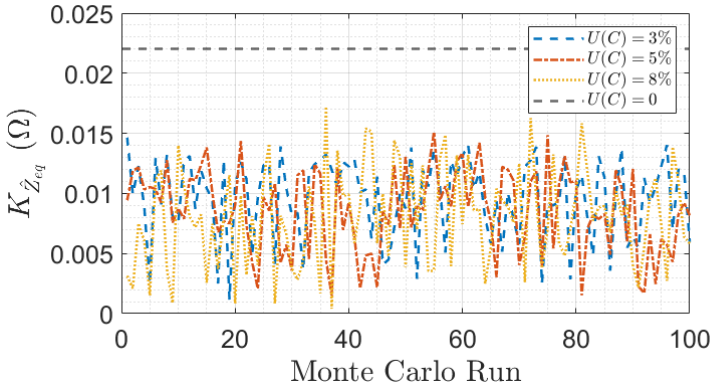

(**a**)

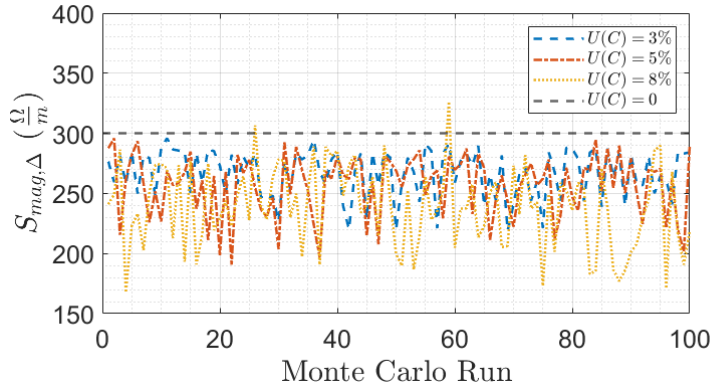

(**b**)

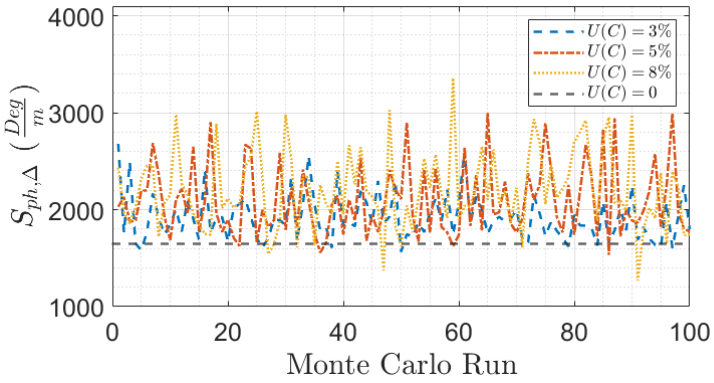

(**c**)

Figure 5. Monte Carlo analysis results: (**a**) $K_{\hat{Z}_{eq}}$ factor, (**b**) sensitivity of magnitude of the input impedance and (**c**) sensitivity of phase of the input impedance.

Overall, none of these consequences significantly compromise the operation of the array sensor, although they slightly deteriorate its performance. It is observed that simulations were carried out with significant deviations of several % to make the results well visible. In real cases, the variability of capacitance and resistance is expected to be in the order of few % (slightly larger for capacitance, e.g., up to 5%), and such variability is intended as a spread of values, so that the associated standard deviation may be considered in the order of 1% to 2%.

Since the $K_{\hat{Z}_{eq}}$ is shown to be variable and smaller than 0.015 Ω (in some cases down to 0.002 Ω), this translates into a requirement for the accuracy of the input impedance measurement, that should ensure a sensitivity of such 2 mΩ to result in an absolutely unaffected position determination. Since the input impedance is measured with a voltamperometric

approach, this translates into a requirement for the voltage and current sensing at the input terminals. Considering $\hat{Z}_{eq}$ values in the order of some Ω (as shown in Figure 4), the uncertainty requirement for the voltage and current measurements is in the order of 0.1%. As anticipated, imposing a variability requirement for capacitance and resistance values of, e.g., 2%, the corresponding voltage and current uncertainty requirement would be shifted to about 0.5%, which is feasible with off-the-shelf sensors.

5.3. Comparison with Other Techniques

The previous discussion has shown that the $K_{\hat{Z}_{eq}}$ value of 0.015 Ω translates into an uncertainty $u\{\hat{Z}_{eq}\} \leq 1\%$, providing a position uncertainty in the order of the 0.1%, as per (16), having $\min_k\{S_{mag}(x_k)\}$ in excess of 100 as per Figure 5b.

Other methods have been proposed in the literature for the position detection of moving objects and we focus on translation movement (rather than rotational, as it occurs for example with motor shafts).

Lim and Kim [29] studied an inductive position sensor (IPS) for automotive applications operating in the MHz range for translational ranges of a tenth of mm. In the studied case, the position range is 12 mm and the resulting accuracy is ±0.85%, including a variation of the air gap of about 2:1 (1.5 mm to 2.5 mm, compared to another sensor based on the 3D Hall effect technology), significantly exceeding ±1%, being often in the order of 5%. The IPS-obtained position accuracy has the same order of magnitude of the estimated impedance uncertainty in our case, to add then the division by the sensitivity function, that reduces thus the error by almost two orders of magnitude.

The localization of an RFID tag is achieved in [21] using magneto-inductive waves at 13.56 MHz. The accuracy is not expressed quantitatively at first, but it is declared acceptable if it is less than the length of one of the cells. In the experimental case then, carried out with 11 cells, the maximum position error at the extremes of the array is about 25% of the cell length, which, compared to our errors, is quite large.

A more classic application to a linear motor is shown in [30], where two-phase magnetic sensing is applied having optimized the phase shift of the two signals. Over a span of ±30 mm, the experimental standard deviation is 1.4 mm as local deviation from the expected linear relationship, so about 2.3%. Wegener et al. [31] reported a similar accuracy of 2.8%.

Golby [32] presented a variant of a linear variable differential transformer with a planar geometry containing three coils: an outer primary rectangular coil and two inner secondary coils with a sine and cosine shape. This device was declared with an accuracy of 0.1% to 1%, although details were not provided.

6. Conclusions

We studied the behavior of resonant arrays used for position measurement of a moving object suitable, in addition to various industrial applications, particularly for DWPT scenarios. The principle of operation of resonator arrays was extensively discussed in [27,28] and has been briefly summarised here. The focus, instead, has been on the accuracy of the position measurement with respect to the variability of the circuit parameters. Structures of coupled resonators in fact may be affected by the uncertainty of the component values.

The parameter mismatch can compromise the performance and operation of the resonator array sensor, as it can make the input impedance non-bijective. The resonator array in fact provides an input impedance curve that depends on the position of the receiver coil and is periodic over the array length, when the receiver passes over each cell (in the complex plane the impedance curve describes concentric circles).

The change in capacitance of tuning capacitors (either by fabrication tolerance or effect of temperature change) affects the value of the resonance frequency, whereas a change in the array coil resistance varies the factor of merit at the resonance, with the risk of

shrinking and collapsing, and making the subsequent loops of the input impedance curve non-distinguishable.

It is clear that the use of precision components for lumped resistors and capacitors is recommended, in order to drastically reduce the uncertainty of the parameters. To limit the mismatch of capacitance from the datasheet value, it is also possible to experimentally select more accurate sets of values, although this operation has a cost. In addition to some optimization of the tuning of resonator array, the Monte Carlo analysis revealed that the effect of capacitance uncertainty is limited and basically leads to a slightly reduced accuracy.

The overall uncertainty of the sensor can also be improved by performing more accurate input current and voltage measurements, once the influence of the coil parameters has been brought in the order of a fraction of %.

Future development of this work is the practical realization of some sensors and verifying their resolution and uncertainty by repeated tests, once systematic errors have been identified and removed. The objective of a practical realization is the demonstration of the parameters relevant to the overall resolution and uncertainty, including fabrication and assembly tolerances, validating the output of the theoretical analysis presented in this paper.

Author Contributions: Conceptualization, M.S., L.S. and A.M.; methodology, A.M.; software, M.S. and L.S.; validation, M.S., L.S. and A.M.; writing—original draft preparation, M.S., L.S. and A.M.; writing—review and editing, M.S., L.S. and A.M.

Funding: This research received no external funding.

Data Availability Statement: The original contributions presented in the study are included in the article, further inquiries can be directed to the corresponding author.

Conflicts of Interest: The authors declare no conflicts of interest.

References

1. Baumer. Robust Ultrasonic Sensors—U500 and UR18. 2024. Available online: https://www.baumer.com/ch/en/product-overview/object-detection/ultrasonic-sensors/product-portfolio/robust-ultrasonic-sensors-with-flexible-parameterization/c/13527 (accessed on 28 July 2024).
2. LION Precision. Comparing Capacitive and Eddy-Current Sensors. 2009. Available online: https://www.lionprecision.com/comparing-capacitive-and-eddy-current-sensors/ (accessed on 29 July 2024).
3. HYDAC. Linear Position Transmitters. 2024. Available online: https://www.hydac.com/shop/en/sensors/linear-position-sensors/linear-position-transmitters (accessed on 29 July 2024).
4. ALTHEN. Linear Position Sensors. 2024. Available online: https://www.althensensors.com/sensors/linear-position-sensors/ (accessed on 29 July 2024).
5. Temposonics. R-Series V Position Sensors. 2024. Available online: https://www.temposonics.com/Products/IndustrialPositionSensors/R-SeriesVPositionSensors (accessed on 28 July 2024).
6. Datlinger, C.; Hirz, M. Benchmark of Rotor Position Sensor Technologies for Application in Automotive Electric Drive Trains. *Electronics* **2020**, *9*, 1063. [CrossRef]
7. Jagiella, M.; Fericean, S.; Dorneich, A. Progress and Recent Realizations of Miniaturized Inductive Proximity Sensors for Automation. *IEEE Sens. J.* **2006**, *6*, 1734–1741. [CrossRef]
8. Webster, J. *The Measurement, Instrumentation and Sensors Handbook*; Springer: Berlin/Heidelberg, Germany, 1999.
9. Pallas-Areny, R.; Webster, J.G. *Sensors and Signal Conditioning*, 2nd ed.; Wiley: Hoboken, NJ, USA, 2012.
10. Jagiella, M.; Fericean, S. Miniaturized inductive sensors for industrial applications. In Proceedings of the IEEE Sensors, Orlando, FL, USA, 12–14 June 2002; Volume 2, pp. 771–778. [CrossRef]
11. Danisi, A.; Masi, A.; Losito, R.; Perriard, Y. Electromagnetic Analysis and Validation of an Ironless Inductive Position Sensor. *IEEE Trans. Instrum. Meas.* **2013**, *62*, 1267–1275. [CrossRef]
12. Jagiella, M.; Fericean, S.; Droxler, R.; Dorneich, A. New magneto-inductive sensing principle and its implementation in sensors for industrial applications. In Proceedings of the IEEE Sensors, Vienna, Austria, 24–27 October 2004; Volume 2, pp. 1020–1023. [CrossRef]
13. Solymar, L.; Shamonina, E. *Waves in Metamaterials*; OUP: Oxford, UK, 2009.
14. Stevens, C.J. Magnetoinductive waves and wireless power transfer. *IEEE Trans. Power Electron.* **2015**, *30*, 6182–6190. [CrossRef]
15. Stevens, C.J. Some consequences of the properties of metamaterials for wireless power transfer. In Proceedings of the 9th International Congress on Advanced Electromagnetic Materials in Microwaves and Optics (METAMATERIALS), Oxford, UK, 7–12 September 2015; pp. 295–297. [CrossRef]

16. Sandoval, F.S.; Moazenzadeh, A.; Wallrabe, U. Comprehensive Modeling of Magnetoinductive Wave Devices for Wireless Power Transfer. *IEEE Trans. Power Electron.* **2018**, *33*, 8905–8915. [CrossRef]
17. Sandrolini, L.; Simonazzi, M.; Barmada, S.; Fontana, N. Two-port network compact representation of resonator arrays for wireless power transfer with variable receiver position. *Int. J. Circuit Theory Appl.* **2022**, *51*, 2301–2314. [CrossRef]
18. Simonazzi, M.; Campanini, A.; Sandrolini, L.; Rossi, C. Design Procedure Based on Maximum Efficiency for Wireless Power Transfer Battery Chargers with Lightweight Vehicle Assembly. *Energies* **2021**, *15*, 70. [CrossRef]
19. Yan, J.; Stevens, C.J.; Shamonina, E. A Metamaterial Position Sensor Based on Magnetoinductive Waves. *IEEE Open J. Antennas Propag.* **2021**, *2*, 259–268. [CrossRef]
20. Herraiz-Martinez, F.J.; Paredes, F.; Zamora Gonzalez, G.; Martin, F.; Bonache, J. Printed Magnetoinductive-Wave (MIW) Delay Lines for Chipless RFID Applications. *IEEE Trans. Antennas Propag.* **2012**, *60*, 5075–5082. [CrossRef]
21. Syms, R.R.A.; Voronov, A.; Sydoruk, O. HF RFID Tag Location Using Magneto-Inductive Waves. *IEEE J. Radio Freq. Identif.* **2022**, *6*, 347–354. [CrossRef]
22. Brecher, A.; Arthur, D. *Review and Evaluation of Wireless Power Transfer (WPT) for Electric Transit Applications*; Technical Report 0060; U.S. Department of Transportation: Washington, DC, USA, 2014.
23. Stepins, D.; Zakis, J.; Kaspars, R.; Husev, O.; Shevchenko, V.; Pakhaliuk, B. Research and Development of Inductive-Resonant Wireless Power Transfer System. In Proceedings of the 2019 IEEE 60th International Scientific Conference on Power and Electrical Engineering of Riga Technical University (RTUCON), Riga, Latvia, 7–9 October 2019. [CrossRef]
24. Low, Z.N.; Chinga, R.A.; Tseng, R.; Lin, J. Design and test of a high-power high-efficiency loosely coupled planar wireless power transfer system. *IEEE Trans. Ind. Electron.* **2009**, *56*, 1801–1812. [CrossRef]
25. Patil, D.; McDonough, M.K.; Miller, J.M.; Fahimi, B.; Balsara, P.T. Wireless Power Transfer for Vehicular Applications: Overview and Challenges. *IEEE Trans. Transp. Electrif.* **2017**, *4*, 3–37. [CrossRef]
26. Pakhaliuk, B.; Husev, O.; Shevchenko, V.; Kroics, K.; Stepins, D.; Strzelecki, R. Automatic Position Detection and Transmitting Activation of Dynamic Wireless Power Transfer System with Air Capacitor. In Proceedings of the 2022 Wireless Power Week (WPW), Bordeaux, France, 5–8 July 2022. [CrossRef]
27. Simonazzi, M.; Sandrolini, L.; Mariscotti, A. Receiver-Coil Location Detection in a Dynamic Wireless Power Transfer System for Electric Vehicle Charging. *Sensors* **2022**, *22*, 2317. [CrossRef] [PubMed]
28. Simonazzi, M.; Sandrolini, L.; Mariscotti, A. Resonator Arrays for Linear Position Sensors. *J. Low Power Electron. Appl.* **2023**, *13*, 41. [CrossRef]
29. Lim, H.S.; Kim, C.Y. ISO26262-Compliant Inductive Long-Stroke Linear-Position Sensors as an Alternative to Hall-Based Sensors for Automotive Applications. *Sensors* **2023**, *23*, 245. [CrossRef] [PubMed]
30. Paul, S.; Chang, J. A New Approach to Detect Mover Position in Linear Motors Using Magnetic Sensors. *Sensors* **2015**, *15*, 26694–26708. [CrossRef] [PubMed]
31. Wegener, R.; Senicar, F.; Junge, C.; Soter, S. Low Cost Position Sensor for Permanent Magnet Linear Drive. In Proceedings of the 2007 7th International Conference on Power Electronics and Drive Systems, Daegu, Republic of Korea, 22–26 October 2007. [CrossRef]
32. Golby, J. Advances in inductive position sensor technology. *Sens. Rev.* **2010**, *30*, 142–147. [CrossRef]